

Theoretical Investigations on the Thermal Decomposition Mechanism of 5-Hydroxy-6-hydroperoxy-5,6-dihydrothymidine in Water

Ze-qin Chen^{†,‡} and Ying Xue^{*,†,§}

College of Chemistry, Key Laboratory of Green Chemistry and Technology in Ministry of Education, Sichuan University, Chengdu 610064, P. R. China, College of Chemistry and Chemical Engineering, China West Normal University, Nanchong 637002, P. R. China, and State Key Laboratory of Biotherapy, Sichuan University, Chengdu 610041, P. R. China

Received: January 31, 2010; Revised Manuscript Received: July 25, 2010

The main primary product of DNA oxidation by free radicals is 5-hydroxy-6-hydroperoxy-5,6-dihydrothymidine (5-OH-6-OOH-DHT), whose further degradation can yield the other mutagenic products and amplify the spectrum of DNA damage. In this study, to illustrate the thermal stability of 5-OH-6-OOH-DHT in DNA, the decomposition mechanism of 5-OH-6-OOH-DHT was identified based on the *cis*-(5*R*,6*S*) diastereomer. Optimized structures for all of the stationary points in the gas phase were investigated at the B3LYP/6-31+G(d,p) level of theory. Four pathways were characterized. The decomposition mechanism of 5-OH-6-OOH-DHT was proposed to involve either dehydration for paths A and B or the cleavage of a glycosidic bond for paths C and D. Moreover, to simulate the title reaction in aqueous solution, a water-mediated mechanism and cluster-continuum model, based on the SCRF/CPCM model, were taken into account. The results indicate that the most favorable reaction pathways for paths A and B both involve a sort of eight-membered ring transition structure formed by two (path A) or one (path B) auxiliary water molecules, suggesting that the thermal decomposition of 5-OH-6-OOH-DHT can be significantly facilitated by water molecules. Path A is the most feasible mechanism reported for the decomposition of 5-OH-6-OOH-DHT in the aqueous solution, which is slightly more favorable than path B. However, the unimolecular decomposition mechanisms (paths C and D) both have high-energy barriers and are largely endothermic, suggesting that the cleavage of the N-glycosidic bond via unimolecular decomposition is thermodynamically and kinetically unfavorable. These studies have shed light on the chemical properties of 5-OH-6-OOH-DHT in free radical reactions and thereby have provided new insights into the complex mechanism of oxidative DNA damage.

1. Introduction

DNA bases are always susceptible to damage by reactive oxygen species (ROS), which is generated by endogenous aerobic respiration and exogenous free-radical-generating agents, such as ultraviolet radiation, ionizing radiation, and chemical species.^{1,2} ROS are the most important cytotoxic and mutagenic agents because they are continuously generated in living cells during normal cellular metabolism and cause a wide variety of oxidative damage to purines and pyrimidines in DNA. Oxidative DNA damage has been considered as an important promoter of cancer, besides being implicated in the normal process of aging, as well as in the etiology of many human diseases, including diabetes, atherosclerosis, and neurodegenerative diseases.^{3–7} The main contributing reactive oxygen species responsible for oxidative DNA damage in biological system appears to be OH radicals generated by radiolytic reactions occurring in water as a result of γ irradiation,⁸ metal ion promoted Fenton-type reaction,⁹ and decomposition reactions of H_2O_2 .¹⁰ Studies have shown that the yield of DNA hydroperoxides by OH radical induced oxidation has been shown to be 50–70% of the total base damage immediately following γ -irradiation of DNA in aqueous aerated solutions.^{11,12} Intact DNA hydroperoxides may

be located on either thymine or cytosine residues since they are unlikely to involve purines which, during radical oxidation, consume relatively low amounts of O_2 and do not form stable hydroperoxides.^{13–15} Therefore, hydroperoxides are the principal intermediates of the free radical induced oxidation of pyrimidines in DNA.

Thymine has been considered as a major target of oxidative base damage, yielding thymine hydroperoxides as primary products.¹⁶ Thymidine hydroperoxides are interesting compounds owing to their relative stability compared to other DNA hydroperoxides.¹⁷ Due to the chirality of the C5 and C6 atoms, thymidine hydroperoxides include eight diastereomers of 5(6)-hydroxy-6(5)-hydroperoxy-5,6-dihydrothymidine and 5-(hydroperoxymethyl)-2'-deoxyuridine (shown in Scheme 1), whose structures and thermal decomposition mechanism have been accomplished thanks to the pioneering work of Wagner et al. through extensive 1H and ^{13}C NMR measurements.¹⁷ A brief mechanism of the formation of thymidine hydroperoxides by OH radical-induced oxidation of thymidine is proposed in Scheme 1. The addition of OH radicals across the C5–C6 pyrimidine double bond of thymidine followed by incorporation of O_2 and subsequent reduction of β -hydroperoxy radicals lead to the formation of thymidine hydroperoxides.^{18–20} Studies have shown that the OH radical shows a 60%:30% preference for adding to the C5 atom of the pyrimidine ring vs the C6 atom, and the remaining (10%) yield deals with the abstraction of a hydrogen atom from the methyl group,¹⁸ which indicates

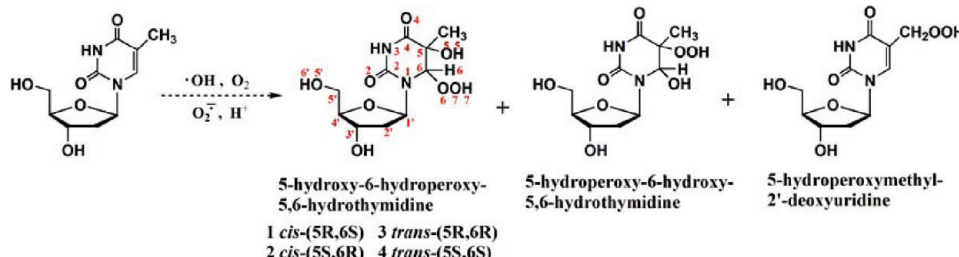
* Corresponding author. E-mail: yxue@scu.edu.cn. Tel.: 86-28-85418330.

† Key Laboratory of Green Chemistry and Technology in Ministry of Education, Sichuan University.

‡ China West Normal University.

§ State Key Laboratory of Biotherapy, Sichuan University.

SCHEME 1: Formation of Thymidine Hydroperoxides by OH Radical Induced Oxidation of Thymidine in Aerated Aqueous Solution



that 5-hydroxy-6-hydroperoxy-5,6-dihydrothymidine (5-OH-6-OOH-DHT) is the major product of OH radical induced oxidation of thymidine. In addition, thymidine hydroperoxides can also be formed by the so-called type I mechanism (one-electron oxidation) upon exposure of DNA to UVA light in the presence of a photosensitizer.^{21,22}

Thymidine hydroperoxides, as a potential source of singlet molecular oxygen in DNA,²³ were known to have mutagenic activities and disrupt cellular homeostasis.²⁴ The further reactions of thymidine hydroperoxides can promote the yields of other degradation products, such as *N*-(2-deoxy-β-D-*erythro*-pentofuranosyl)-5-hydroxy-5-methylbarbituric acid, *N*-(2-deoxy-β-D-*erythro*-pentofuranosyl)-5-hydroxy-5-methylhydantoin, and 5-(hydroxymethyl)-2'-deoxyuridine, etc., and amplify the spectrum of DNA damage. This makes it imperative to investigate the thermal stability of thymidine hydroperoxides in DNA. However, to the best of our knowledge, there are few data on the thermal decomposition mechanism of thymidine hydroperoxides at the theory level up to now. Studies have implied that the mechanism of decomposition is the same for thymidine hydroperoxides which are attached to DNA or which are free in solution.¹⁷ Then, to illuminate the fate of the major thymidine hydroperoxide, 5-OH-6-OOH-DHT, in DNA, we have optimized its structure and investigated its decomposition mechanism in aqueous solution not only for its unimolecular decomposition reaction but also for its water-mediated mechanism with one, two, and three water molecules in some appropriate steps and further utilized the conductor-like polarized continuum model (CPCM) to evaluate the solvent effects on the main pathway based on the density functional theory (DFT) B3LYP method. 5-OH-6-OOH-DHT has drawn special interest due to its greater yield than the other two types of thymidine hydroperoxides and lack of a systematic study in the literature.²¹ For 5-OH-6-OOH-DHT, there are four diastereomers, i.e., *cis*-(5R,6S) **1**, *cis*-(5S,6R) **2**, *trans*-(5R,6R) **3**, and *trans*-(5S,6S) **4** forms, whose general structures and atom labeling are illustrated in Scheme 1. It should be noted that the atoms on the pyrimidine ring have the same labeling as the atoms directly connected with them. So, to denote an atom unambiguously, the name of an atom consists of two parts: the name of the element followed by the atom labeling. Considering the similarity in the decomposition mechanism of the four diastereomers (**1–4**), the thermal decomposition of 5-OH-6-OOH-DHT was studied based on the *cis*-(5R,6S) diastereomer model, which was found to be the most stable both by our theoretical calculation and by experimental result.¹⁷

2. Computational Details

The structures of minima and transition states were fully optimized using the density functional theory (DFT) employing a hybrid functional of B3LYP,^{25,26} thanks to its successful

application in the DNA nucleoside hydrolysis,^{27,28} the hydrolysis and aminolysis of amide^{29–32} and esters,^{33–35} and other analogous systems,^{36–38} with a standard 6-31+G(d,p) basis set. The harmonic frequency analysis was used to confirm the stationary point as a minimum with all positive frequencies or as a transition state with only one imaginary frequency. The connectivity between the stationary points was established by intrinsic reaction coordinate (IRC) calculations.^{39,40} Although diffuse functions have been shown to be required to properly describe anionic hydrogen-bonded systems, the use of diffuse functions on larger models becomes increasingly computationally expensive. As our goal is to adequately depict the decomposition mechanism of 5-OH-6-OOH-DHT in aqueous solution, it would be beneficial to identify a reduced basis set with equal accuracy. Therefore, Figures S1 and S2 in the Supporting Information compare the B3LYP geometries of the reactant (RE), transition state (TS), and product complex (PC) for the direct decomposition pathway optimized with the 6-31+G(d,p) and 6-311++G(2d,p) basis sets, while Tables S1 compares the energy barriers and reaction energies calculated using both basis sets. The results clearly indicate that the geometries and corresponding energetics are not highly dependent on the basis set used in the geometry optimization. Therefore, our discussion mainly focuses on the 6-31+G(d,p) geometries and energies.

In the case of the solvent effect, in our model, a local microhydration surrounding was simulated with one to three water molecules around the reaction centers. At the same time, the bulk solvent effect of water was also tested by single-point calculation at the geometry optimization level by means of the conductor-like polarized continuum model (CPCM), which has prevailed in the scientific community due to its high validity and the relative simplicity of the expressions involved in the definition of the solvent reaction field.^{41,42} This hybrid solvation model (the local microhydration–continuum model) has been successfully utilized in a number of organic reactions.^{34,36,38} The dielectric constant used in the calculations is $\epsilon = 78.4$ for water. Note that all of the single-point energies in water were corrected by the gas-phase thermodynamic quantities. All calculations were performed by the Gaussian 03 program.⁴³

3. Results and Discussion

3.1. Structural Features of 5-OH-6-OOH-DHT. A geometry optimization for the four diastereomers (**1–4**) of 5-OH-6-OOH-DHT was carried out on the whole structure, without any constraints, at the B3LYP/6-311++G(2d,p) level, which contains enough diffuse functions to gain more accurate structural parameters and energies. The computational structural features and relative energies are presented in Figure 1.

(1) Pyrimidine Ring. The pyrimidine ring of 5-OH-6-OOH-DHT exhibits a half chair conformation geometry as already

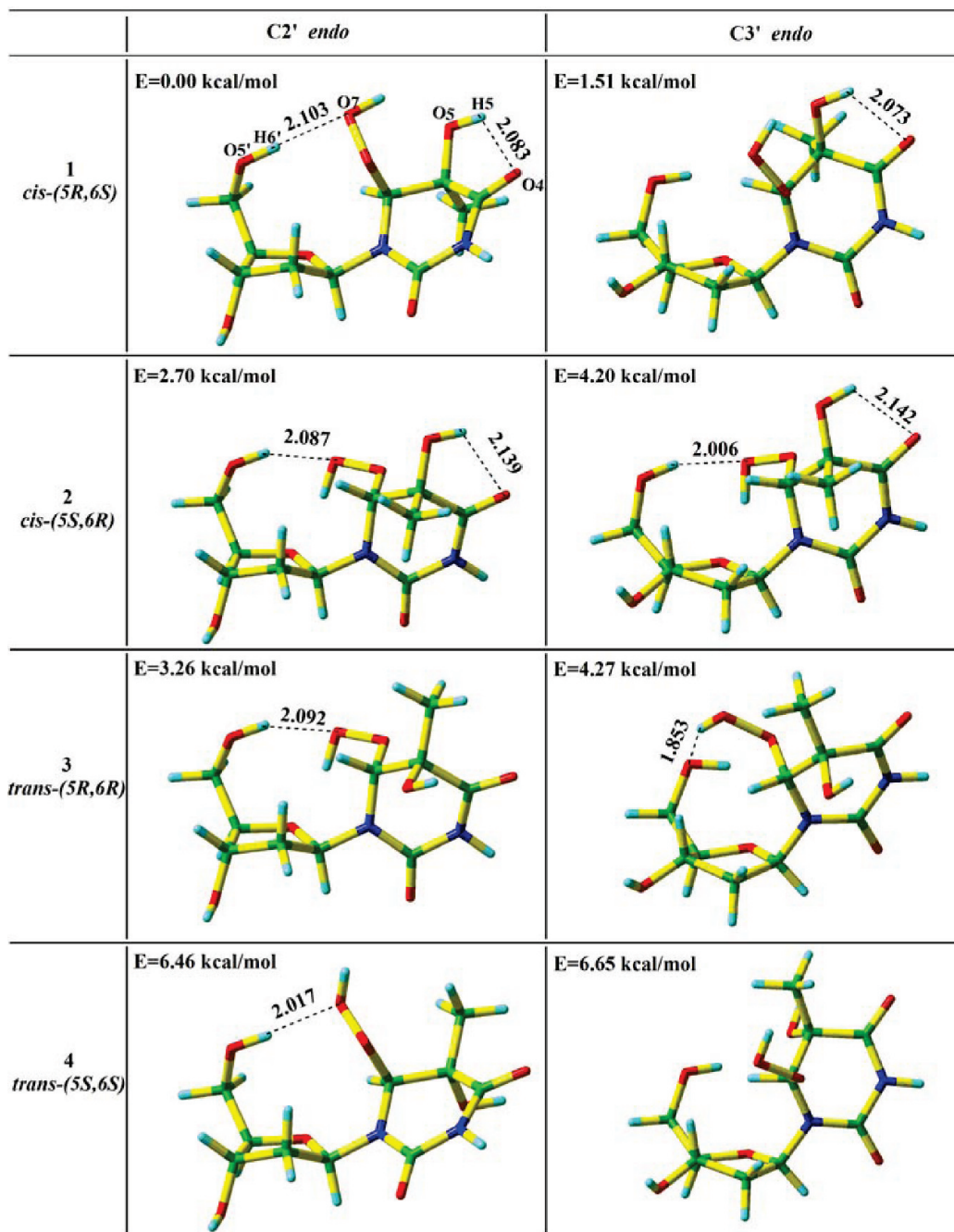
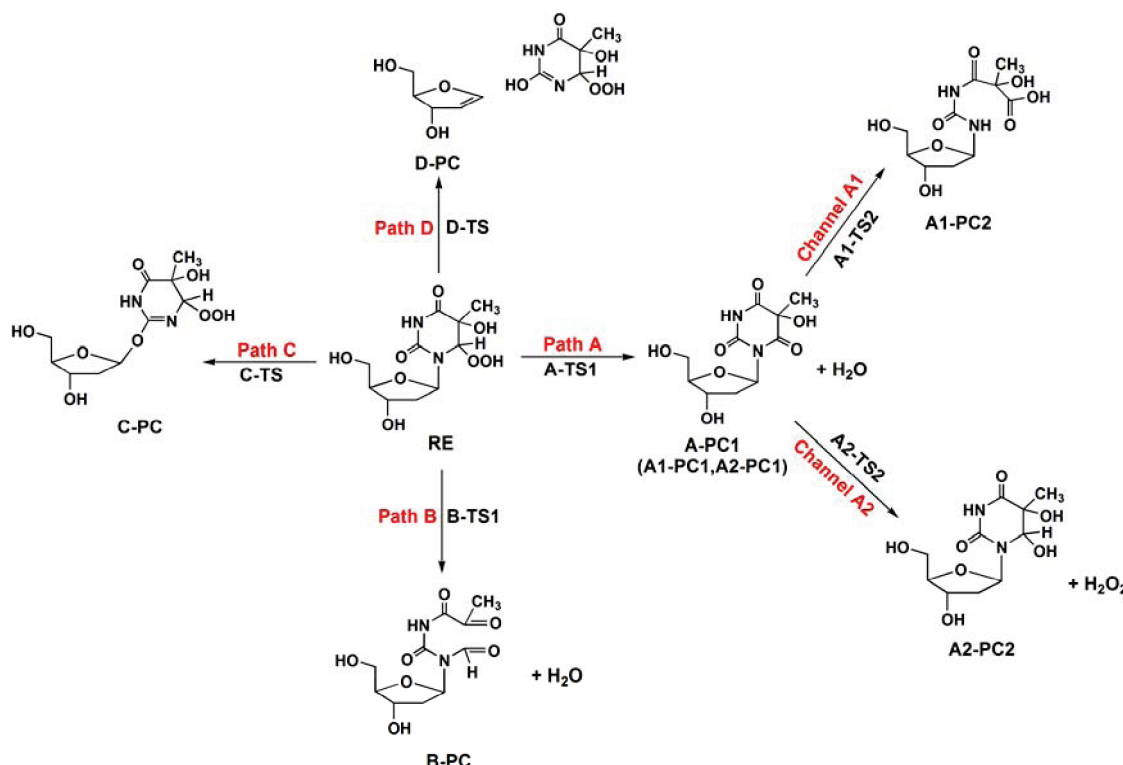


Figure 1. Structural features and relative energies for the four diastereomers (**1–4**) of 5-OH-6-OOH-DHT in two possible sugar packings at the B3LYP/6-311++G(2d,p) level of theory (the energy of *cis*-(5*R*,6*S*) is set to zero).

described for 5,6-saturated 2,4-dioxopyrimidine derivatives.^{44–47} The best four-atom mean plane is defined by N1, C2, N3, and C4 atoms. The pyrimidine ring adopts four preferential puckered conformations in the gas phase, in which the C6 hydroperoxy substitutes are always axial with respect to the pyrimidine ring, whereas the C5 hydroxy substitutes may be either axial or equatorial, depending on whether the diastereomer is *cis* or *trans*. For the *cis* diastereomers (**1** and **2**), the C5 methyl group occupies axial position and the C5 hydroxy group is equatorial with the pyrimidine ring, i.e., coplanar with the C₄=O group, which allows the formation of the strong intramolecular hydrogen bond (O5–H…O4). In contrast, the positions of C5 methyl and hydroxy groups in *trans* diastereomers (**3** and **4**) are contrary to those in *cis* diastereomers: the C5 hydroxy group is axial and out of the C₄=O plane, and the C5 methyl group

locates at equatorial position. Then, no intramolecular hydrogen bond is formed in the *trans* diastereomers.

(2) **Sugar Moiety.** Usually, the furanose ring conformation of nucleosides in DNA is described in terms of a dynamic equilibrium between two C2' *endo* and C3' *endo* puckered forms. To obtain the most stable sugar conformation of 5-OH-6-OOH-DHT, both of the sugar packings were optimized with the same stereochemistry of base. As depicted in Figure 1, for C2' *endo*, the hydroperoxy group at the C6 atom to some extent always interacts with the exocyclic hydroxymethyl moiety, leading to the formation of a strong intramolecular hydrogen bond (O5'–H…O7). In C3' *endo*, however, the intramolecular hydrogen interaction only occurs in the *cis*-(5*S*,6*R*) and *trans*-(5*R*,6*R*) diastereomers. In point of the energy, the energy of each C2' *endo* packing is lower than its counterpart in C3' *endo*

SCHEME 2: Possible Reaction Pathways for the Decomposition of 5-OH-6-OOH-DHT

packing. This result indicates that C2' *endo* is the most stable sugar packing for 5-OH-6-OOH-DHT, whose stability is mainly attributed to the cocontribution of the sugar ring and the intermolecular hydrogen bond (O5'-H \cdots O7).

For C2' *endo* sugar packing, the four diastereomers display a notable difference in their stability with the *cis* diastereomers (**1** and **2**) being more stable than *trans* diastereomers (**3** and **4**). The order of the stability of hydroperoxides **1–4** (*cis* > *trans*) appears to be related to the presence of intramolecular interaction (O5-H \cdots O4), which just exists in the *cis* diastereomers (**1** and **2**). The stabilities of the four diastereomers at room temperature are similar to those of thymidine glycol, *cis*-(5*R*,6*S*) > *cis*-(5*S*,6*R*) > *trans*-(5*R*,6*R*) > *trans*-(5*S*,6*S*).

In summary, the structure features presented here for the four diastereomers of 5-OH-6-OOH-DHT agree well with the experimental structures.¹⁷ Therefore, it seems that the B3LYP approach is acceptable for this work.

3.2. Direct Decomposition Mechanism of *cis*-(5*R*,6*S*) Diastereomer. As mentioned above, among the four diastereomers of 5-OH-6-OOH-DHT, the *cis*-(5*R*,6*S*) conformer is the most stable and is chosen as the reaction system. Four possible pathways were considered, designated as paths A, B, C, and D (Scheme 2). For 5-OH-6-OOH-DHT, the main decomposition pathways in water have been established on the basis of the isolation and identification of the intermediates and final oxidation products.¹⁷ Three products, a large amount of *N*-(2-deoxy- β -D-*erythro*-pentofuranosyl)-5-hydroxy-5-methylbarbituric acid (A-PC1) and *N*¹-(2-deoxy- β -D-*erythro*-pentofuranosyl)-N³-tartronoylurea (A1-PC2) as well as a trace amount of thymidine glycol (A2-PC2), were identified in the experiment. The formation of these products is consistent with initial dehydration of the C6 hydroperoxide group giving rise to A-PC1 (step 1 of path A), which may undergo subsequent hydrolysis into A1-PC2 (channel A1 of path A) or A2-PC2 (channel A2 of path A). Apart from path A, another dehydration mechanism was also characterized in our calculation, which is a direct ring-

opening mechanism, leading to the formation of a ring-opening product B-PC. In addition, the other two mechanisms involving the cleavage of the N-glycosidic bond were depicted by paths C (direct cleavage pathway) and D (abstraction cleavage pathway), respectively.

3.2.1. Path A. (1) *A-Step 1.* The optimized geometries and important bond lengths for the stationary points in the first step of path A are shown in Figure 2a. As shown in Figure 2a, a four-membered transition state A-TS1 is located in our calculation. The distances of C6-H6, H6-O7, O7-O6, and O6-C6 are 1.252, 1.506, 1.961, and 1.303 Å, respectively. The transfer of the proton (H6) toward the O7 atom leads to an elongation of 0.163 Å for C6-H6 bond length and a reduction of 0.140 Å for the C6-O6 bond in contrast to those of the A-RE. The vector of the imaginary vibrational frequency for the transition state A-TS1 mainly corresponds to the proton (H6) transfer from C6 to O7 atoms. As the reaction proceeds, the first product A-PC1 is formed. For the geometry of A-PC1, the hybridization of the C6 atom converts from sp^3 in A-RE to sp^2 . The distance of C6-O6 is 1.214 Å, shorter than those in A-RE and A-TS1 by 0.229 and 0.089 Å, respectively, suggesting that the C6-O6 bond in A-PC1 becomes stronger and changes from the single bond in A-RE into a double bond. The released water molecule remains coordinated to the sugar moiety and pyrimidine through two strong hydrogen bonds, O7-H \cdots O6 and O5'-H \cdots O7.

(2) *A-Step 2.* Starting from A-PC1, the reaction may keep going to yield two other hydrolytic products (A1-PC2 and A2-PC2) via two channels in the subsequent step, denoted as channels A1 and A2, respectively. In channel A1, the nucleophilic attack of one water molecule at the C6 atom and the simultaneous proton transfer to the N1 atom result in the cleavage of the C6-N1 bond. In channel A2, a tetrahedral product, thymidine glycol, is generated by the addition of the C6=O6 double bond by two protons, which come from two different water molecules. The optimized geometries and

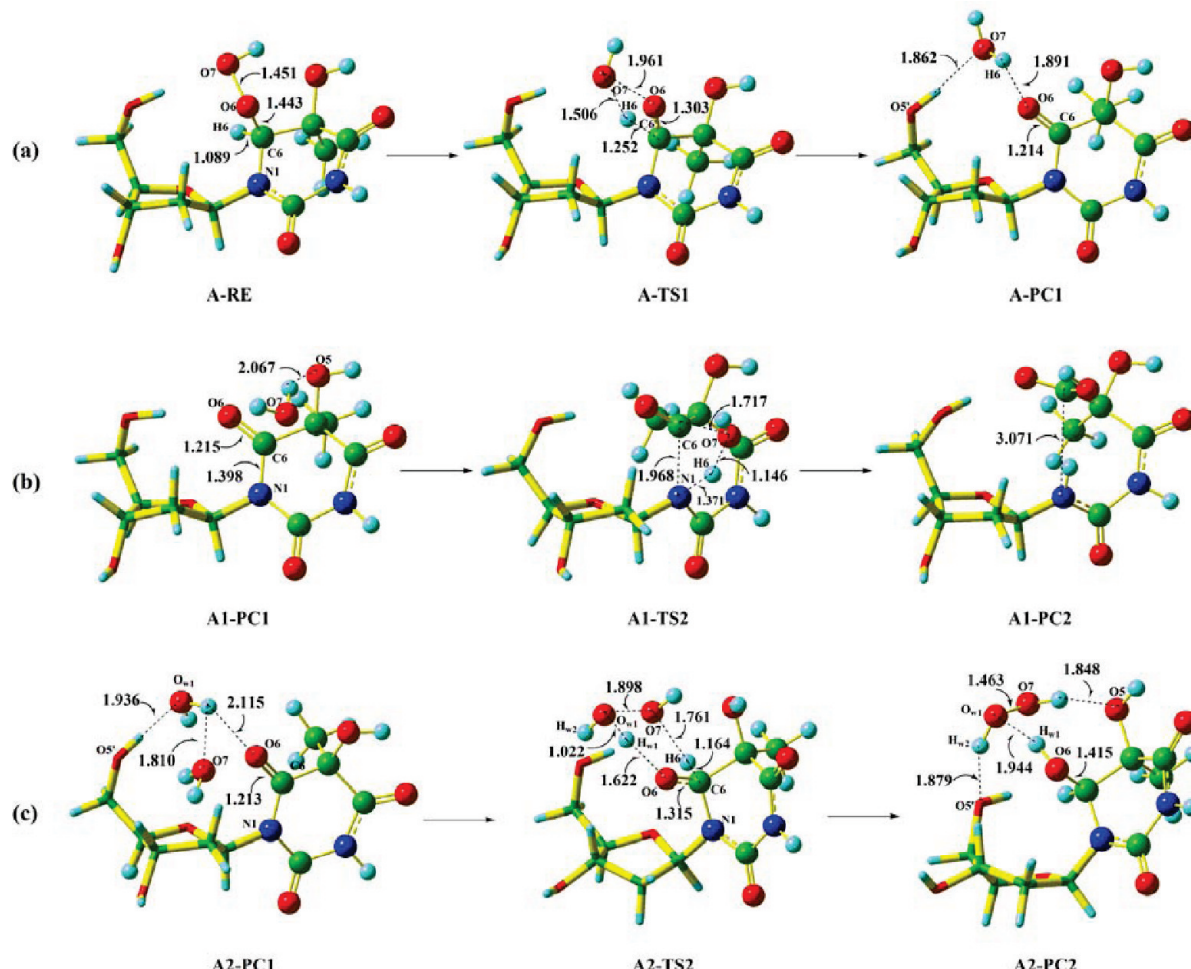


Figure 2. Optimized structures of the stationary points for path A at the B3LYP/6-31+G(d,p) level (bond length in angstroms).

important bond lengths for the stationary points of channels A1 and A2 are shown in (b) and (c) of Figure 2, respectively.

Channel A1. This pathway is associated with A1-PC1.⁴⁸ As described in Figure 2b, A1-PC1 is generated due mainly to the H-bond network, where the water molecule is connected by a hydrogen bond ($O_7-H\cdots O_5$). The reaction, involving the nucleophilic attack of the O_7 atom of a water molecule to the C_6 atom and the simultaneous proton (H_6) transfer from the water molecule to the N_1 atom, is concerted via the transition state A1-TS2. The transition state A1-TS2 is also a four-membered ring structure. The vector of the imaginary vibrational frequency of the transition state is mainly associated with the motion of the proton (H_6) from O_7 to N_1 atoms, leading to the partial cleavage of the C_6-N_1 bond. The C_6-N_1 bond length of A1-TS2 is 1.968 Å, elongated by 0.570 Å as compared to that of A1-PC1 (1.398 Å). The distances of N_1-H_6 , H_6-O_7 , and O_7-C_6 are 1.371, 1.146, and 1.717 Å, respectively. The final ring-opening product A1-PC2 is obtained after surmounting the transition state A1-TS2, in which the O_7 atom is certainly bound to the C_6 atom and the H_6 atom is fully transferred to the N_1 atom. The long length of C_6-N_1 bond in A1-PC2 is 3.071 Å, longer than those in A1-PC1 and A1-TS2 by 1.673 and 1.103 Å, respectively, which confirms the complete cleavage of the C_6-N_1 bond.

Channel A2. This process is associated with A2-PC1.⁴⁹ As shown in Figure 2c, in A2-PC1, three strong hydrogen bonds, $O_{w1}-H\cdots O_7$, $O_5'-H\cdots O_{w1}$, and $O_{w1}-H\cdots O_6$, constitute the H-bond network and connect the two water molecules, sugar moiety, and pyrimidine together. The transition state A2-TS2

is a six-membered ring structure. IRC results show that this step is associated with the coupling model of the H_6 and H_{w1} atoms' simultaneous transfer from the two water molecules to the $C_6=O_6$ bond, leading to the formation of thymidine glycol and H_2O_2 . The distances of C_6-H_6 , H_6-O_7 , O_7-O_{w1} , $O_{w1}-H_{w1}$, and $H_{w1}-O_6$ are 1.164, 1.761, 1.898, 1.022, and 1.622 Å, respectively. The length of the C_6-O_6 bond is elongated by about 0.102 Å from A2-PC1 (1.213 Å) to A2-TS2 (1.315 Å), suggesting that the $C_6=O_6$ double bond becomes weaker in the transition state. After the transition state A2-TS2 is overcome, the product A2-PC2 is produced. In A2-PC2, the hybridization of the C_6 atom converted from sp^2 in A2-PC1 to sp^3 . The length of the C_6-O_6 bond is 1.415 Å, 0.202 Å longer than that in A2-PC1, which suggests that the C_6-O_6 has evolved from a double bond in A2-PC1 into a single bond. The released H_2O_2 molecule interacts with the sugar moiety and pyrimidine through three strong hydrogen bonds, $O_7-H\cdots O_5'$, $O_6-H\cdots O_{w1}$, and $O_{w1}-H\cdots O_5'$.

3.2.2. Path B. In analogy to path A, path B also involves the dehydration of the C_6 hydroperoxide group, giving rise to a ring-opening product B-PC. However, it is not the H_6 atom but the H_5 atom that is transferred. The optimized geometries and important bond lengths for the stationary points are shown in Figure 3. As depicted in Figure 3, the transition state B-TS is a six-membered ring structure, whose vibrational model is mainly associated with the transfer of the proton (H_5) from O_5 to O_7 atom with the simultaneous breakages of C_5-C_6 and O_6-O_7 bonds. The distances of C_5-O_5 , O_5-H_5 , H_5-O_7 , O_7-O_6 , O_6-C_6 , and C_6-C_5 are 1.342, 1.044, 1.427, 1.975,



Figure 3. Optimized structures of the stationary points for path B at the B3LYP/6-31+G(d,p) level (bond length in angstroms).

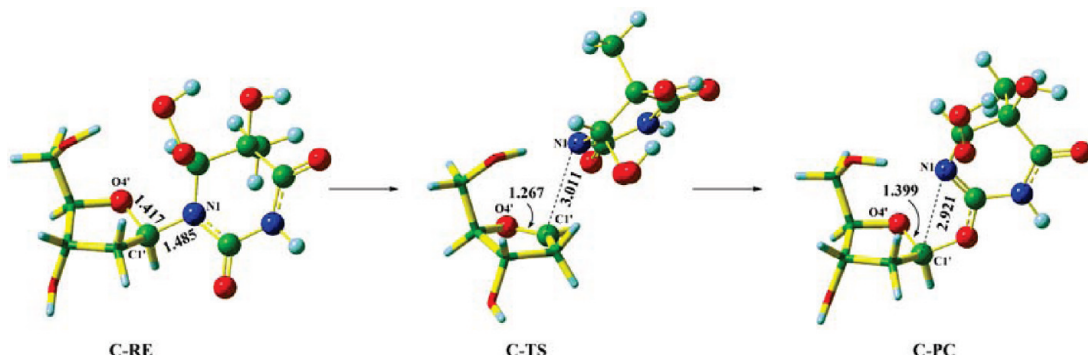


Figure 4. Optimized structures of the stationary points for path C at the B3LYP/6-31+G(d,p) level (bond length in angstroms).

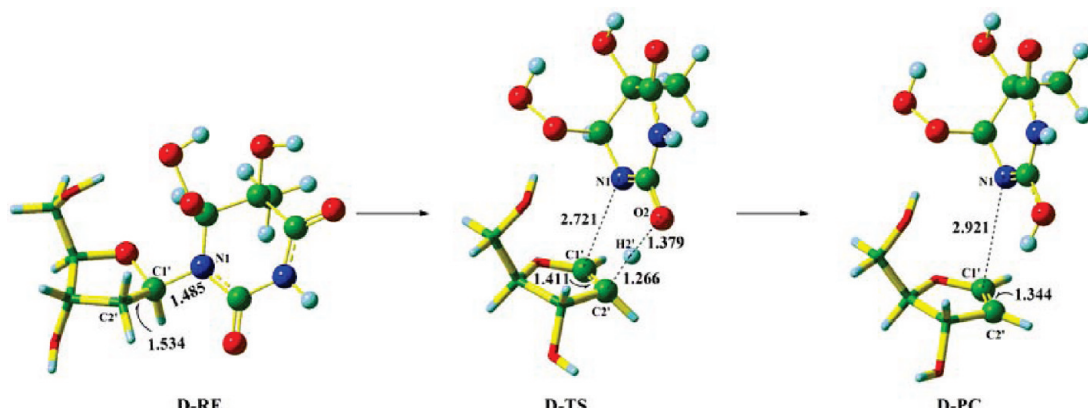


Figure 5. Optimized structures of the stationary points for path D at the B3LYP/6-31+G(d,p) level (bond length in angstroms).

1.298, and 1.781 Å, respectively. The bond angle of O5–H5–O7 is 157.20°, which deviates slightly from a line, and the H5 atom can effectively head toward the lone pairs of the O7 atom. Therefore, the transition state B-TS is a favorable structure for this decomposition process. As the reaction proceeds, the ring-opening product B-PC is formed. In B-PC, the lengths of C5=O5 and C6=O6 double bonds are 1.220 and 1.217 Å, respectively, shorter than those in B-RE by 0.204 and 0.226 Å, respectively, which shows that both of the bonds have changed from the single bond in B-RE into a double bond, and the hybridization of C5 and C6 atoms converts from sp^3 in B-RE to sp^2 .

3.2.3. Path C. All the optimized structures of the reactant, transition state, and product are presented in Figure 4. The vector of the imaginary vibrational frequency of the transition state C-TS mainly corresponds to the cleavage of the C1’–N1 bond. The length of the C1’–N1 bond in C-TS is 3.011 Å, longer than those in the reactant C-RE (1.485 Å), indicating that the N-glycosidic bond has almost been cleaved in the transition state. The hybridization of C1’ converts from sp^3 in C-RE to sp^2 , and the C1’–O4’ single bond changes into a double bond (1.417 Å in C-RE vs 1.267 Å in C-TS). Due to the instability of the (charge) separated sugar cation and base anion in the

gas phase, the pyrimidine ring rotates to coordinate O2 to the C1’ atom following the cleavage of the glycosidic bond, leading to the formation of the C1’–O2 bond in the product. In C-PC, the C1’–O4’ single bond is restored (1.399 Å in C-PC).

3.2.4. Path D. Further searches of the potential energy surface for the unimolecular decomposition reaction reveal the second possible transition state. The optimized geometries and important bond lengths for the stationary points are shown in Figure 5. The vibrational model for the transition state D-TS mainly corresponds to the proton (H2’) transfer from C2’ to O2 atoms, which is favorable in the gas phase to stabilize a partial negative charge on the base and a partial positive charge on the sugar. An elongation of 0.236 Å for the C1’–N1 bond length from D-RE (1.485 Å) to D-TS (2.721 Å) confirms the partial cleavage of the N-glycosidic bond in D-TS. In the transition state, the hydrogen atom H2’—which is the transferred atom—is almost equidistant between C2’ (1.266 Å) and O2 (1.379 Å) atoms. The distance of C1’–C2’ is 1.411 Å, shorter than that in the reactant D-RE (1.534 Å), indicating that the C1’–C2’ bond becomes stronger in D-TS because of the partial cleavages of the C1’–N1 and C2’–H2’ bonds. In the product D-PC, the hybridizations of the C1’ and C2’ atoms convert from sp^3 in D-RE to sp^2 , leading to the formation of a C1’=C2’ bond (1.344

TABLE 1: Changes of Gibbs Free Energies (ΔG) and Electronic Energies (ΔE) for the Direct Decomposition Mechanism of *cis*-(5R,6S)-5-OH-6-OOH-DHT in the Gas Phase and Aqueous Solution (in kcal/mol)

	$\Delta G(\text{gas})$	$\Delta G(\text{sol})$	$\Delta E(\text{gas})$	$\Delta E(\text{sol})$
Path A				
A-RE→A-TS1	49.03	45.99	49.47	46.43
A-RE→A-PC1	-70.64	-74.45	-68.20	-72.01
A1-PC1→A1-TS2	52.62	50.41	50.62	48.42
A1-PC1→A1-PC2	5.87	3.97	5.48	3.59
A2-PC1→A2-TS2	133.29	139.20	130.70	136.61
A2-PC1→A2-PC2	71.19	75.48	70.37	74.07
Path B				
B-RE→B-TS	33.41	31.22	33.64	31.45
B-RE→B-PC	-55.15	-59.33	-49.01	-53.18
Path C				
C-RE→C-TS	38.84	32.70	39.40	33.26
C-RE→C-PC	19.63	17.86	19.96	18.20
Path D				
D-RE→D-TS	36.65	34.07	37.25	34.68
D-RE→D-PC	23.34	22.20	25.87	24.73

\AA in D-PC), which flattens the sugar ring. The nucleobase remains coordinated to the sugar moiety through a weak interaction with the newly formed C1'-C2' double bond in D-PC.

The changes in Gibbs free energies (ΔG) and electronic energies (ΔE) for the direct decomposition mechanism of *cis*-(5*R*,6*S*)-5OH-6-OOH-DHT are given in Table 1. The corresponding calculated total relative energy profiles are presented in Figure 6. As depicted in Figure 6a, the free energy barriers of paths A, B, C, and D are 49.03, 33.41, 38.84, and 36.65 kcal/mol, respectively, in the gas phase, which correspond to 45.99, 31.22, 32.70, and 34.07 kcal/mol, respectively, in the aqueous solution. It is clear from our calculation that the presence of the solvent water to some extent contributes to lower all the energy barriers. Both paths A and B are largely exothermic (with reaction energies of 40–80 kcal/mol). For path A, starting from the initial stable product A-PC, another two products A1-PC2 and A2-PC2 may be formed. From the potential energy profile shown in Figure 6b, it can be seen that the Gibbs free energy barrier of A1-TS2 and A2-TS2 is 52.62 and 133.29 kcal/mol, respectively, in the gas phase, which correspond to 50.41 and 139.20 kcal/mol in the aqueous solution, respectively. The free energy barrier of A2-TS2 is so high that

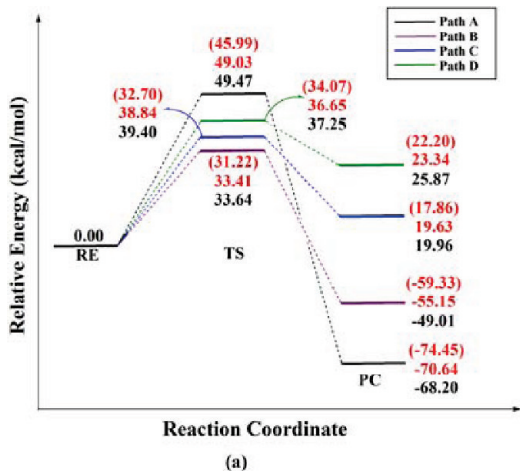
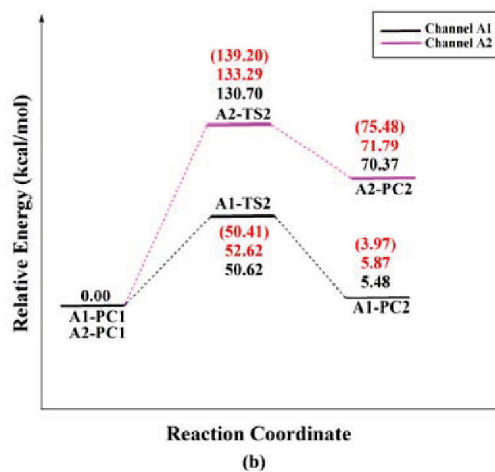


Figure 6. Potential energy profiles for the direct decomposition mechanism of *cis*-(5*R*,6*S*)-5OH-6-OOH-DHT. (Bottom value, ΔE in the gas phase; middle value, ΔG in the gas phase; top value in parentheses, ΔG in aqueous solution. Definitions are the same in the following figures.)

TABLE 2: Changes of Gibbs Free Energies (ΔG) and Electronic Energies (ΔE) for the Water-Mediated Mechanism of *cis*-(5R,6S)-5-OH-6-OOH-DHT in the Gas Phase and Aqueous Solution (in kcal/mol)

	$\Delta G(\text{gas})$	$\Delta G(\text{sol})$	$\Delta E(\text{gas})$	$\Delta E(\text{sol})$
Path A				
Single-Water-Mediated Decomposition Mechanism				
1W-A-RC \rightarrow RE + H ₂ O	2.15	8.01	-6.40	-0.55
1W-A-RC \rightarrow 1W-A-TS1	38.34	37.50	36.81	35.99
1W-A-RC \rightarrow 1W-A-PC1	-68.70	-72.15	-67.43	-70.88
1W-A1-PC1 \rightarrow RE + H ₂ O	-67.61	-64.42	-73.74	-70.54
1W-A1-PC1 \rightarrow 1W-A1-TS2	50.97	45.37	46.43	40.82
1W-A1-PC1 \rightarrow 1W-A1-PC2	7.95	3.52	8.10	3.67
Two-Water-Mediated Decomposition Mechanism				
2W-A-RC \rightarrow RE + 2H ₂ O	8.93	22.62	-8.72	4.96
2W-A-RC \rightarrow 2W-A-TS1	33.52	29.16	31.98	27.63
2W-A-RC \rightarrow 2W-A-PC1	-78.87	-81.37	-77.04	-79.54
2W-A1-PC1 \rightarrow RE + 2H ₂ O	-66.89	-57.87	-81.99	-72.96
2W-A1-PC1 \rightarrow 2W-A1-TS2	48.82	43.21	43.73	38.11
2W-A1-PC1 \rightarrow 2W-A1-PC2	2.61	6.56	0.77	4.72
Three-Water-Mediated Decomposition Mechanism				
3W-A-RC \rightarrow RE + 3H ₂ O	5.89	24.60	-19.05	-0.33
3W-A-RC \rightarrow 3W-A-TS1	36.58	31.84	34.40	29.66
3W-A-RC \rightarrow 3W-A-PC1	-72.79	-74.28	-72.01	-73.51
3W-A1-PC1 \rightarrow RE + 3H ₂ O	-70.76	-51.86	-94.59	-75.69
3W-A1-PC1 \rightarrow 3W-A1-TS2	53.65	43.35	48.98	38.68
3W-A1-PC1 \rightarrow 3W-A1-PC2	5.80	6.85	4.60	5.65
Path B				
Single-Water-Mediated Decomposition Mechanism				
1W-B-RC \rightarrow RE + H ₂ O	8.72	11.90	0.81	4.00
1W-B-RC \rightarrow 1W-B-TS1	30.55	30.26	29.43	29.14
1W-B-RC \rightarrow 1W-B-IM	-60.74	-61.80	-56.36	-57.42
Two-Water-Mediated Decomposition Mechanism				
2W-B-RC \rightarrow RE + 2H ₂ O	8.01	19.54	-9.31	2.23
2W-B-RC \rightarrow 2W-B-TS1	34.02	31.20	33.80	30.97
2W-B-RC \rightarrow 2W-B-IM	-57.89	-57.90	-54.66	-54.66

it is rather difficult for channel A2 to occur. Clearly, in the kinetic point, the formation thymidine glycol is not feasible in our results, which is in agreement with experimental results that thymidine hydroperoxides do not undergo hydrolytic cleavage to give H_2O_2 and thymidine glycol.¹⁷ The high yield of thymidine glycol in some previous studies^{50,51} may likely be attributed to metal-catalyzed reactions since no precautions were taken to eliminate metal ions from the decomposition solutions. For example, the addition of μM Fe^{2+} to γ -irradiated DNA immediately reduces the level of intact hydroperoxides by about 50%, probably leading to the formation of thymidine glycol.^{52,53} Even so, large free energy barriers are still involved in path A, which mainly arises from the four-centered transition states



ism of *cis*-(5R,6S)-5OH-6-OOH-DHT. (Bottom value, ΔE in the gas phase aqueous solution. Definitions are the same in the following figures.)

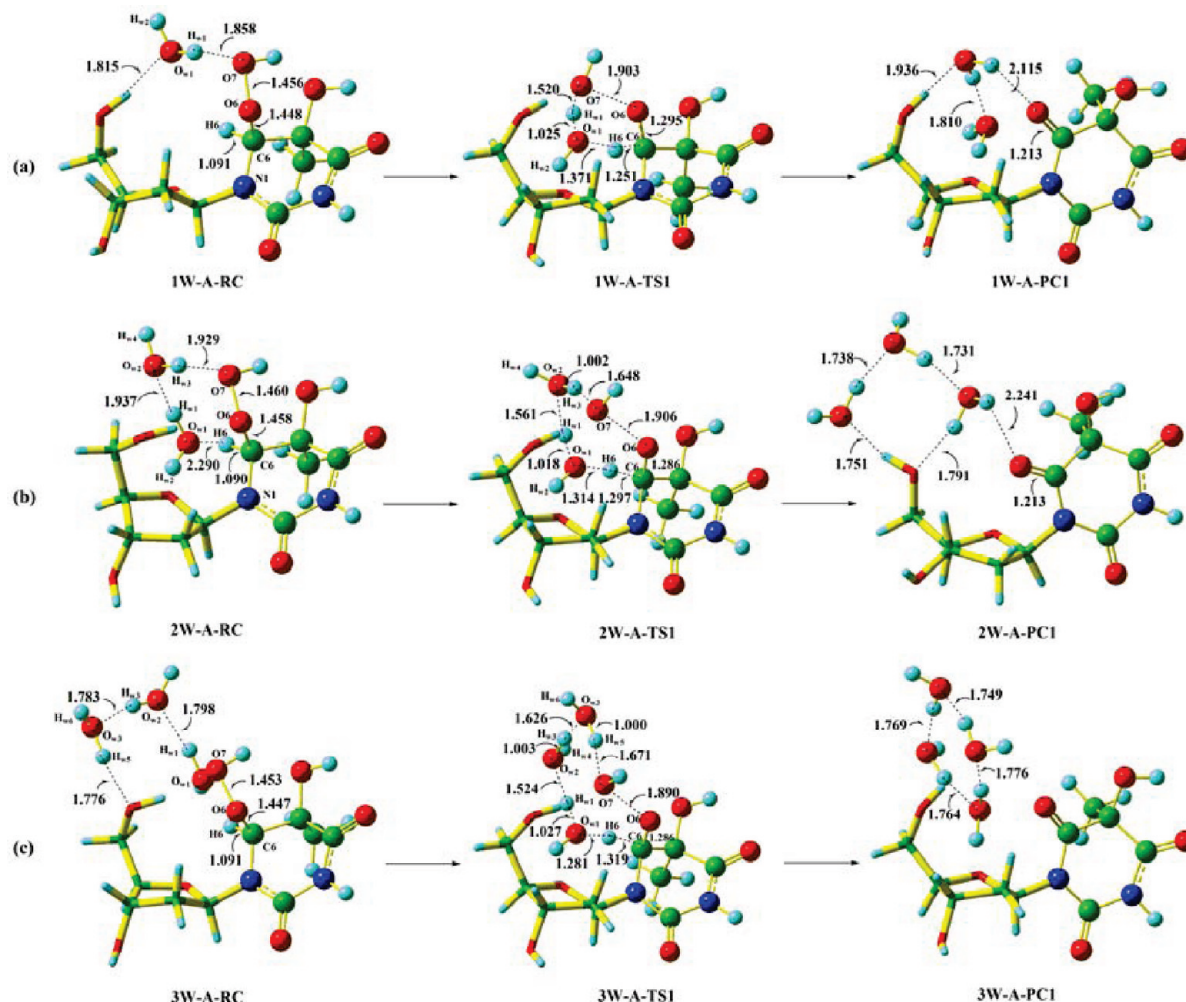


Figure 7. Optimized structures of the stationary points in the water-mediated mechanisms of A-step 1 with one (a), two (b), and three (c) water molecules at the B3LYP/6-31+G(d,p) level (bond length in angstroms).

A-TS1 and A1-TS2. In such cyclic transition states, the orbits required for the bond dissociation and formation are deformed so much that a large amount of deformation energy is needed. Moreover, the bulk solvation contributes slightly to lowering the energy barrier. Then, to relax these transition states and reduce the angle strain, we further investigated the water-mediated mechanisms.

3.3. Water-Mediated Decomposition Mechanism. In this part, to obtain the most stable transition state with the least ring constraint, the water-mediated decomposition mechanisms of paths A and B are clarified with one to three water molecules. To conveniently state the water-mediated mechanism, the names of stationary structures in the water-mediated mechanism are further modified with the prefixes *n*W, in which the letter W implies the participation of an auxiliary water molecule and *n* is the number of the auxiliary water molecules. For instance, the term 1W-A1-TS2 represents the transition state of channel A1 for the single-water-mediated mechanism. In addition, it should be noted that the same atom numbering may not be the same atom in different figures herein and hereafter. The changes in Gibbs free energies (ΔG) and electronic energies (ΔE) for the water-mediated mechanism are presented in Table 2.

3.3.1. Path A. (1) A-Step 1. In this step, we have explored the water-mediated mechanisms including one, two, and three water molecules, respectively. The corresponding optimized structures of the reactant complexes (RCs), transition states, and

product complexes and the calculated relative energy profiles are presented in Figures 7 and 8, respectively.

For the single-water-mediated decomposition reaction, the auxiliary water molecule acts as a proton bridge, receiving a proton and donating one in turn. As depicted in Figure 7a, attributed to the presence of the auxiliary water molecule, transition state 1W-A-TS1 is a six-membered ring structure. The IRC result indicates that 1W-A-TS1 is concerted but asynchronous because the cleavage of the C6–H6 bond is previous to the formation of the O7–H_{w1} bond. The distances of C6–O₆, O₆–O₇, O₇–H_{w1}, H_{w1}–O_{w1}, O_{w1}–H₆, and H₆–C₆ are 1.295, 1.903, 1.520, 1.025, 1.371, and 1.251 Å, respectively. The analysis of the vibrational frequency of the transition state indicates that it mainly corresponds to the coupling of the transfer of the H₆ atom from C₆ to O_{w1} atoms and the transfer of the H_{w1} atom from O_{w1} to O₇ atoms, leading to the cleavage of the O₆–O₇ bond. After checking the transition state 1W-A-TS1, we find that the bond angles C6–H6–O_{w1} (162.48°) and O_{w1}–H_{w1}–O₇ (152.10°) deviate slightly from a line, and the H₆ and H_{w1} atoms can effectively head toward the lone pairs of O_{w1} and O₇ atoms. Therefore, the transition state 1W-A-TS1 is more favorable than the strained transition state A-TS1 in the direct decomposition mechanism. According to the energy data in Figure 8a, the binding energy of 1W-A-RC was 6.40 kcal/mol in the gas phase, while the Gibbs free energy for the formation of 1W-A-RC is 2.15 kcal/mol including the contribu-

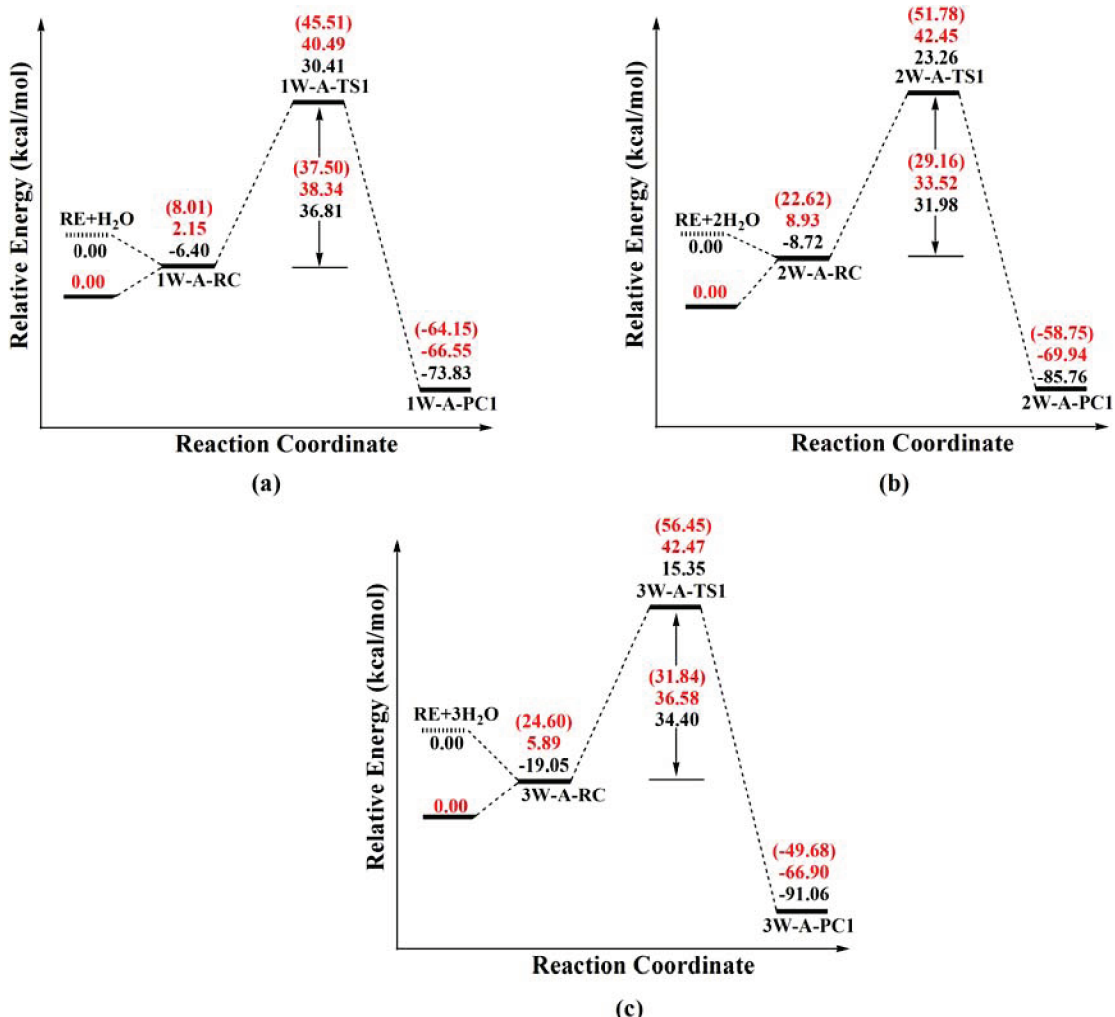


Figure 8. Potential energy profiles for the water-mediated mechanisms of A-step 1 with one (a), two (b), and three (c) water molecules.

tion of entropies. Taking into account the solvent effect, the relative Gibbs free energy of 1W-A-RC increases to 8.01 kcal/mol at the CPCM-B3LYP/6-31+G(d,p) level. The free energy barriers for the single-water-mediated mechanism are 38.34 and 37.50 kcal/mol from 1W-A-RC to 1W-A-TS1 in the gas phase and aqueous solution, respectively, which, as expected, are decreased drastically by ca. 10 kcal/mol in comparison with those of the direct reaction process due to the contribution of one-water-bridge. This result exhibits that the auxiliary water molecule involving the dehydration reaction is thermodynamically and kinetically favorable both in the gas-phase and in aqueous solution. The formation of the favored six-membered ring structure in the transition state leads to the reduction of the ring constraint for the proton transfer, and most of the energy saving has been achieved for its small deformation. To further reduce the ring constraint, one more water was added to act as a bridge to transfer protons.

With two auxiliary water molecules bridging H6 and O7 atoms, the located transition state 2W-A-TS1 is an eight-membered ring structure, which is directly associated with the coupling of the transfer of the H6 atom from C6 to O_{w1} atoms, the transfer of the H_{w1} atom from O_{w1} to O_{w2} atoms, and the transfer of H_{w3} from O_{w2} to O7 atoms. The degree of proton transfer of H6 atom is higher than those of H_{w1} and H_{w3} atoms. As depicted in Figure 7b, compared with 1W-A-TS1, the C6–H6 distance in 2W-A-TS1 remarkably elongates to 1.297 Å with the simultaneous reduction of the C6–O6 bond (1.286

Å). The distances of O6–O7, O7–H_{w3}, H_{w3}–O_{w2}, O_{w2}–H_{w1}, H_{w1}–O_{w1}, and O_{w1}–H₆ are 1.906, 1.648, 1.002, 1.561, 1.018, and 1.314 Å, respectively. Less strain is also observed in the eight-membered ring 2W-A-TS1, in which three hydrogen bonds (C6–H6–O_{w1}, O_{w1}–H_{w1}–O_{w2}, O_{w2}–H_{w3}–O7) exist with angles of 160.1°–172.7°, obviously better than those in the 1W-A-TS1, implying that more relaxed geometry in 2W-A-TS1 clearly favors the triple proton transfer compared with 1W-A-TS1. We deemed that 2W-A-TS1 might be a rational and favored geometry because protons or hydrogen atoms more effectively headed toward lone pairs with a little angle constraint. In this process, as shown in Figure 8b, the binding energy of 2W-A-RC is 8.72 kcal/mol in the gas phase. The free energy barrier was 33.52 and 29.16 kcal/mol from 2W-A-RC to 2W-A-TS1 in the gas phase and aqueous solution, respectively, which are 5–8 kcal/mol lower than those of 1W-A-TS1. This suggests that the eight-centered structure 2W-A-TS1 facilitates the proton transfer and energy saving owing to its smaller deformation than the six-centered structure.

As the next logical step, the effect of a third water molecule on step 1 is considered. As our goal is to get the most stable transition state structure with the least ring constraint, we here mainly discuss the placement of the third water molecule at the site of proton transfer, thus expanding the proton-transfer ring to ten atoms. As shown in Figure 7c, 3W-A-TS1 is a ten-membered ring structure. The imaginary frequency is mainly associated with the coupling of the transfer of the H6 atom from

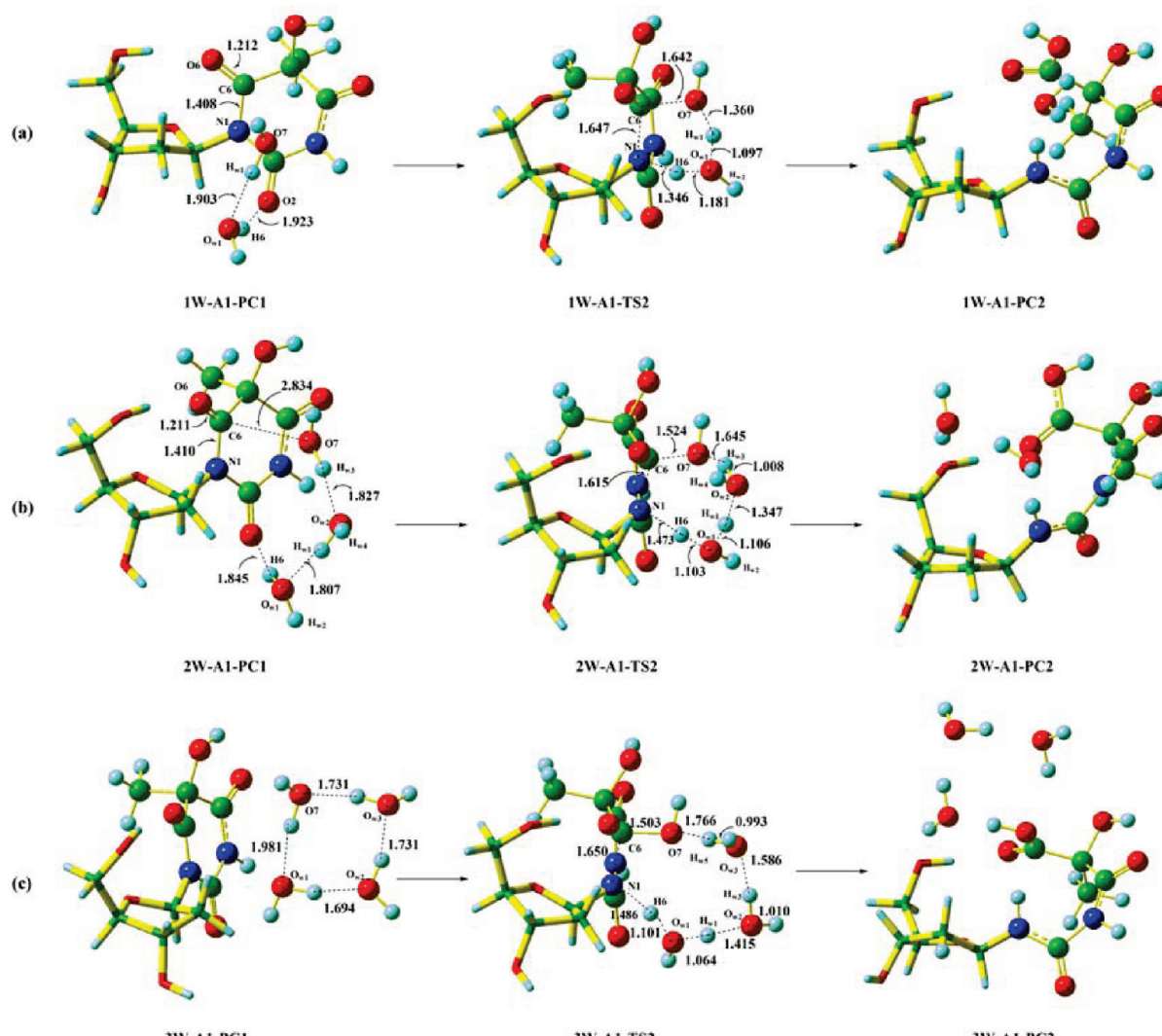


Figure 9. Optimized structures of the stationary points in the water-mediated mechanisms of A-channel A1 with one (a), two (b), and three (c) water molecules at the B3LYP/6-31+G(d,p) level (bond length in angstroms).

C6 to O_{w1} atoms, the transfer of the H_{w1} atom from O_{w1} to O_{w2} atoms, and the transfer of H_{w3} from O_{w2} to O_{w3} atoms as well as the transfer of the H_{w5} atom from O_{w3} to O7 atoms. The distances of C6–O6, O6–O7, O7–H_{w5}, H_{w5}–O_{w3}, O_{w3}–H_{w3}, H_{w3}–O_{w2}, O_{w2}–H_{w1}, H_{w1}–O_{w1}, O_{w1}–H6, and C6–H6 are 1.286, 1.890, 1.671, 1.000, 1.626, 1.003, 1.524, 1.027, 1.281, and 1.319 Å, respectively. The calculated binding energy of 3W-A-RC depicted in Figure 8c is 19.05 kcal/mol in the gas phase. The free energy barriers of 3W-A-TS1 are 36.58 and 31.84 kcal/mol from 3W-A-RC in the gas phase and aqueous solution, respectively, which are about 2 kcal/mol higher than those of 2W-A-TS1, implying that expanding the transition state structure from an eight-membered to a ten-membered ring if one more water is engaged in the proton transfer process can not further lower the energy barrier in both the gas phase and aqueous solution. These results indicate that (i) the ten-membered ring transition state structure 3W-A-TS1 is less favorable than the eight-membered ring 2W-A-TS1 and (ii) the two-water-mediated mechanism is the most favorable reaction route for the dehydration process, whose activation energy (27.63 kcal/mol) is close to the experimental value (ca. 24 kcal/mol).

(2) *A-Channel A1.* For channel A1 of step 2, the water-mediated reaction mechanisms including one, two, and three water molecules were investigated one by one. The optimized geometries and important bond lengths for the stationary points

and the relative energy profiles are presented in Figures 9 and 10, respectively.

As stated previously, A1-TS2 is a four-membered cycle structure. We also added one more water molecule as a bridge to reduce the ring constraint. Figure 9a shows that the transition state 1W-A1-TS2 is a six-membered cycle structure. The imaginary frequency is mainly associated with the coupling of the shift of the H6 atom from O_{w1} to N1 atoms, the H_{w1} atom from O7 to O_{w1} atoms, and the addition of O7 to C6 atoms, resulting in the breakage of the C6–N1 bond. The distances of C6–N1, N1–H6, H6–O_{w1}, O_{w1}–H_{w1}, H_{w1}–O7, and O7–C6 in 1W-A1-TS2 are 1.647, 1.346, 1.181, 1.097, 1.360, and 1.642 Å, respectively. Because of the proton transfer, the C6–N1 bond length in 1W-A1-TS2 is obviously elongated by 0.239 Å with respect to 1W-A1-PC1 (1.408 Å). The bond angles N1–H6–O_{w1} and O_{w1}–H_{w1}–O7 in 1W-A1-TS2 are 160.51 and 150.14°, respectively, suggesting that less strain is involved in the six-membered ring transition state 1W-A1-TS2 than that in the four-membered ring transition state A1-TS2 with the bond angle N1–H6–O7 of 137.09°. The energy data in Figure 10a show that the free energy barriers of 1W-A1-TS2 are 50.97 and 45.37 kcal/mol in the gas phase and aqueous solution, respectively, which are 2–5 kcal/mol lower than those in the direct hydrolysis reaction. This may also be attributed to the fact that there is a less strained six-membered ring transition state in the

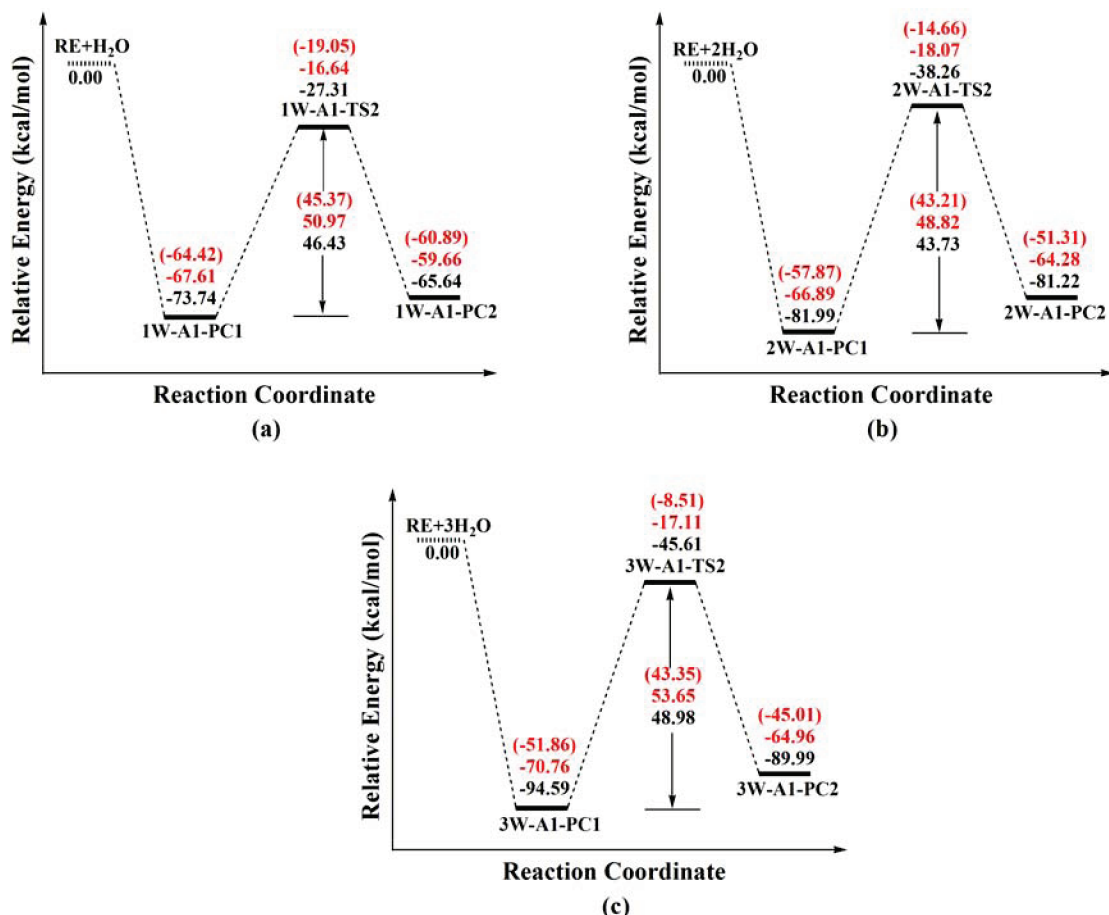


Figure 10. Potential energy profiles for the water-mediated mechanism of A-channel A1 with one (a), two (b), and three (c) water molecules.

one-water-mediated hydrolysis instead of the high strained four-membered ring transition state in the direct hydrolysis process.

In analogy to step 1, a second water molecule was also added to further reduce the ring constraint in the subsequent calculation. Figure 9b illustrates that the transition state 2W-A1-TS2 is an eight-membered ring structure due to the two-water-bridge. The vector of the imaginary vibrational frequency for the transition state mainly corresponds to the coupling of the transfer of H₆ from the O_{w1} atom to the N₁ atom, the transfer of H_{w1} from the O_{w2} atom to the O_{w1} atom, the transfer of the H_{w3} atom from the O₇ atom to the O_{w2} atom, and the addition of the O₇ atom to the C₆ atom. The distances of C₆–N₁, N₁–H₆, H₆–O_{w1}, O_{w1}–H_{w1}, H_{w1}–O_{w2}, O_{w2}–H_{w3}, and H_{w3}–O₇ are 1.615, 1.473, 1.103, 1.106, 1.347, 1.008, and 1.645 Å, respectively. Interestingly, we also found that this process includes an OH anion in nature, in which the H_{w3} atom slightly transfers from O_{w2} to O₇ atoms. The distance of O₇–C₆ in 2W-A1-TS2 is 1.524 Å, shorter than that in A1-TS2 and 1W-A1-TS2 by 0.193 and 0.118 Å, respectively, indicating that the O₇ atom can effectively distribute the electron density to the C₆ atom. That is, it was favorable for the O₇ atom to have a nucleophilic attack on the C₆ atom. As shown in Figure 10b, the free energy barrier of 2W-A1-TS2 is 48.82 kcal/mol from 2W-A1-PC1 in the gas phase, which decreases to 43.21 kcal/mol in the aqueous solution. The increment from the six-membered ring structure 1W-A1-TS2 to the eight-membered ring structure 2W-A1-TS2 relaxes the strain slightly in the geometry of the hydrogen bonds, leading to a small reduction of the free energy barrier (2 kcal/mol) for 2W-A1-TS2 as compared to that of 1W-A1-TS2. The converged free energy barriers of 2W-A1-TS2 indicate that the

eight-membered ring transition state structure 2W-A1-TS2 is slightly more favorable than the six-membered ring 1W-A1-TS2.

As far as the effect of a third water molecule is concerned, to avoid wordy discussion, the geometries of the stationary points (shown in Figure 9c) involved in the three-water-mediated mechanism have not been discussed in detail any more. Emphasis is placed on the energetics (depicted in Figure 10c). As presented in Figure 10c, the free energy barrier of 3W-A1-TS2 is 53.65 kcal/mol in the gas phase, which decreases to 43.35 kcal/mol in aqueous solution. Compared to 2W-A1-TS2, the free energy barrier of 3W-A1-TS2 has been increased by 0.14 kcal/mol in aqueous solution, indicating that the ten-membered ring transition state 3W-A1-TS2 is not more favorable than eight-membered ring transition state 2W-A1-TS2. Therefore, the most favorable reaction route for the ring-opening reaction also involves two water molecules via the eight-membered ring transition state.

3.3.2. Path B. For path B, the water-mediated reaction mechanisms including one and two water molecules were investigated in sequence. The optimized geometries and important bond lengths for the stationary points and the relative energy profiles are presented in Figures 11 and 12, respectively.

Due to the presence of the one-water-bridge, the transition state of path B changes from the six-membered ring structure in B-TS into an eight-membered cycle structure in 1W-B-TS. The vector of the imaginary vibrational frequency for 1W-B-TS mainly corresponds to the coupling of the transfer of the H₅ atom from O₅ to O_{w1} atoms and the transfer of the H_{w1} atom from O_{w1} to O₇ atoms. The distances of C₅–C₆, C₆–O₆,

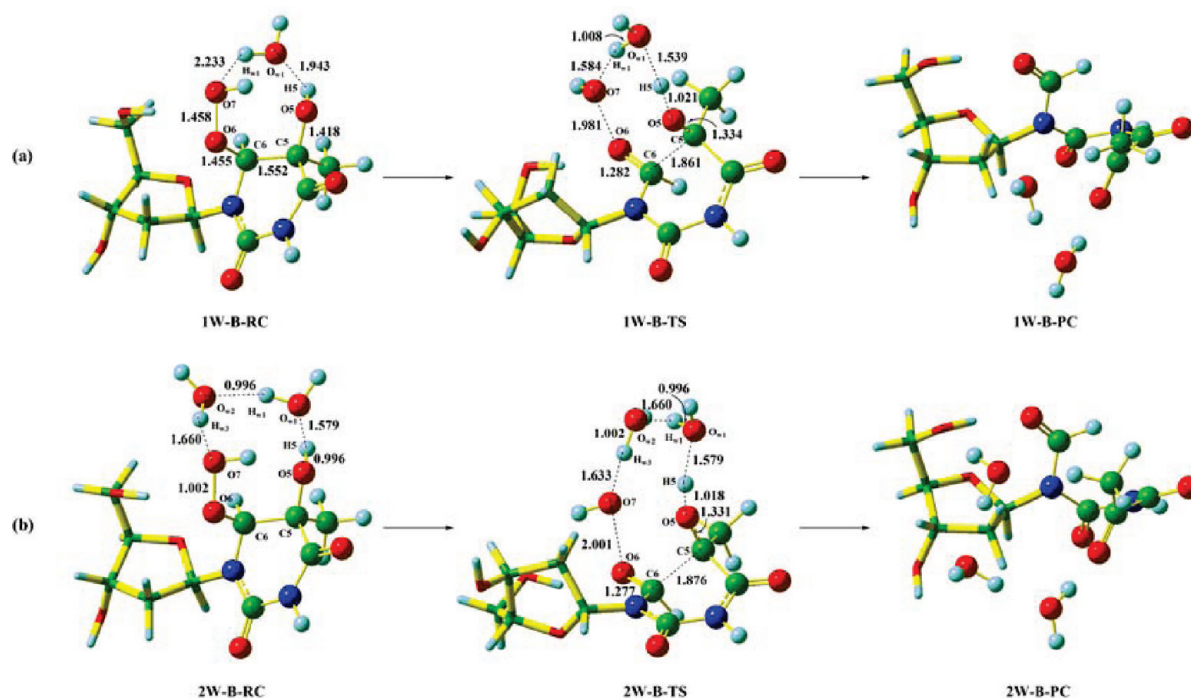


Figure 11. Optimized structures of the stationary points in the water-mediated mechanisms of path B with one (a) and two (b) water molecules at the B3LYP/6-31+G(d,p) level (bond length in angstroms).

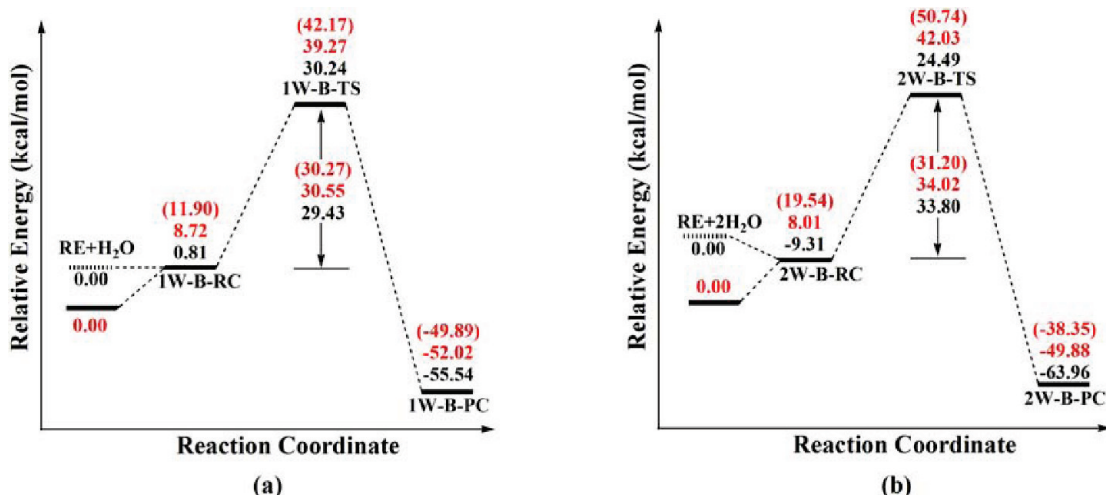


Figure 12. Potential energy profiles for the water-mediated mechanism of path B with one (a) and two (b) water molecules.

O₆—O₇, O₇—H_{w1}, H_{w1}—O_{w1}, O_{w1}—H₅, H₅—O₅, and O₅—C₅ are 1.861, 1.282, 1.981, 1.584, 1.008, 1.539, 1.021, and 1.334 Å, respectively. The bond angles C₅—H₅—O_{w1} (174.93°) and O_{w1}—H_{w1}—O₇ (154.52°) deviate a little from a line, and the H₅ and H_{w1} atoms can effectively head toward the lone pairs of O_{w1} and O₇ atoms. According to the energy data in Figure 12a, the binding energy of 1W-B-RC is 0.81 kcal/mol in the gas phase, while the Gibbs free energy for the formation of 1W-B-RC is 8.72 kcal/mol in the gas phase and 11.90 kcal/mol in aqueous solution. The free energy barriers for the single-water-mediated mechanism of path B are 30.55 and 30.26 kcal/mol from 1W-B-RC to 1W-B-TS in the gas phase and aqueous solution, respectively, which are decreased slightly by 2 kcal/mol in comparison with those of the direct decomposition mechanism, suggesting that slight strain in the geometry of the hydrogen bonds has been relaxed in the eight-membered ring structure 1W-B-TS, leading to a small reduction of free energy barrier.

Subsequently, one more water molecule was also added to expand the proton-transfer ring. As shown in Figure 11b, the transition state 2W-B-TS is a ten-membered cycle structure. The analysis of the vibrational frequency of the transition state indicates that it mainly corresponds to the coupling of the transfer of the H₅ atom from C₅ to O_{w1} atoms, the transfer of the H_{w1} atom from O_{w1} to O_{w2} atoms, and of the H_{w3} atom from O_{w2} to O₇ atoms, leading to the cleavage of the C₅—C₆ bond. The calculated binding energy of 2W-B-RC shown in Figure 12b is 9.31 kcal/mol in the gas phase. The free energy barriers of 2W-B-TS are 34.02 and 31.20 kcal/mol from 2W-B-RC in the gas phase and aqueous solution, respectively, which are 1–3 kcal/mol higher than those of 1W-B-TS, implying that expanding the transition state structure from an eight-membered to a ten-membered ring structure can not further decrease the energy barrier in both the gas phase and aqueous solution. Consequently, the eight-membered ring transition state structure 1W-

B-TS is the most favorable reaction route for the direct ring-opening reaction.

Taking into account the four pathways, it can be seen that, for an aqueous solution, the free energy barriers of the four pathways from the reactant complex obey the following order: path A < path B < path C < path D. Apart from this, paths C and D are both largely endothermic (with reaction energies of 17–26 kcal/mol). The reverse free energy barriers of paths C and D are 11.87 and 14.84 kcal/mol in the aqueous solution, which are 22.20 and 17.86 kcal/mol lower than those in the forward reaction, respectively. Therefore, the reaction equilibrium of paths C and D strongly lost the balance toward reactant, implying that the cleavage of the N-glycosidic bond via unimolecular decomposition is not feasible. Consequently, it is clear that paths A and B both have the high possibility to occur in the aqueous solution, and path A is slightly more favorable than path B.

4. Conclusions

Thymidine hydroperoxides are the primary products of DNA oxidation by free radicals. The thermal decomposition mechanism of 5-OH-6-OOH-DHT, a main thymidine hydroperoxide, was studied at the B3LYP/6-31+G(d,p) level based on the most stable *cis*-(5*R*,6*S*) diastereomer. Two types of reaction processes were taken into account in our calculation. One is the dehydration mechanism (paths A and B), and the other is the cleavage mechanism of the N-glycosidic bond (paths C and D). For the former, both the direct and the water-mediated mechanisms were investigated. The results indicate that the most favorable reaction pathways for paths A and B both involve a sort of eight-membered ring transition structure. The catalytic effects of water molecules owing to the alleviation of ring strain in the proton transfer process may result from the synergistic effects of rehybridization or charge reorganization from the prereaction complex to the transition state structure induced by water molecules. Path A is the most feasible mechanism reported for the decomposition of 5-OH-6-OOH-DHT in the aqueous solution, and the next one is path B. Our studies have shed light on the chemical properties of 5-OH-6-OOH-DHT in free radical reactions and thereby have provided new insights into the complex mechanism of oxidative DNA damage.

Acknowledgment. This project has been supported by the National Natural Science Foundation of China (Grant Nos. 20773089 and 20835003) and the Scientific Research Foundation for the Returned Overseas Chinese Scholars, State Education Ministry (Grant No. 20071108-18-15).

Supporting Information Available: Selected B3LYP/6-31+G(d,p) and B3LYP/6-311++G(2d,p) geometrical parameters for the direct decomposition mechanism of the *cis*-(5*R*,6*S*) diastereomer and comparison of the barriers and reaction energies calculated using the B3LYP/6-31+G(d,p) and B3LYP/6-311++G(2d,p) geometries for the direct decomposition mechanism. Listings of optimized Cartesian coordinates and energies of all stationary points along the potential energy profile in hartree at the B3LYP/6-31+G(d,p) and B3LYP/6-311++G(2d,p) levels. This material is available free of charge via the Internet at <http://pubs.acs.org>.

References and Notes

- Halliwell, B.; Gutteridge, J. M. C. *Methods Enzymol.* **1990**, *186*, 1–85.
- Ames, B. N.; Shigenaga, M. K.; Hagen, T. M. *Proc. Natl Acad. Sci. U.S.A.* **1993**, *90*, 7915–7922.
- Marnett, L. J. *Carcinogenesis* **2000**, *21*, 361–370.
- Olsinski, R.; D. Gackowski, M.; Fokinska, R.; Rozalski, K.; Roszowska; Jaruga, P. *Free Radical Biol. Med.* **2002**, *33*, 192–200.
- Collins, A. R.; Duthie, S. J.; Fillion, L.; Gedik, C. M.; Vaughan, N.; Wood, S. G. *Biochem. Soc. Trans.* **1997**, *25*, 326–31.
- Das, U. N. *Med. Sci. Monit.* **2002**, *8*, 79–92.
- Jackson, A. L.; Loeb, L. A. *Mutat. Res.* **2001**, *477*, 7–21.
- Teoule, R. *Int. J. Radiat. Biol.* **1987**, *51*, 573–589.
- Goldstein, S.; Meyerstein, D.; Czapski, G. *Free Radical Biol. Med.* **1993**, *15*, 435–445.
- Lagercrantz, C. *J. Am. Chem. Soc.* **1973**, *95*, 220–225.
- Schweibert, M. C.; Daniels, M. *Int. J. Radiat. Phys. Chem.* **1971**, *3*, 353–336.
- Michaels, H. B.; Hunt, J. W. *Anal. Biochem.* **1978**, *87*, 135–140.
- Willson, R. L. *Int. J. Radiat. Biol.* **1970**, *27*, 349–358.
- Isilidir, M.; Schuchman, M. N.; Schulte-Froehlinde, D.; von Sonntag, C. *Int. J. Radiat. Biol.* **1982**, *42*, 525–533.
- Bothe, E.; Behrens, G.; Bohm, E.; Sethuram, B.; Schulte Froehlinde, D. *Int. J. Radiat. Biol.* **1986**, *49*, 57–66.
- Cadet, J.; Di Mascio, P. *Peroxides in Biological Systems*; Wiley: Hoboken, NJ, 2006.
- Wagner, J. R.; Van Lier, J. E.; Berger, M.; Cadet, J. *J. Am. Chem. Soc.* **1994**, *116*, 2235–2242.
- Jovanovic, S. V.; Simic, M. G. *J. Am. Chem. Soc.* **1986**, *108*, 5968–5972.
- Wagner, J. R.; van Lier, J. E.; Decarroz, C.; Cadet, J. *Bioelectrochem. Bioenerg.* **1987**, *18*, 155–162.
- Wagner, J. R.; van Lier, J. E.; Johnston, L. *J. Photochem. Photobiol.* **1990**, *52*, 333–343.
- Delatour, T.; Douki, T.; D'Ham, C.; Cadet, J. *J. Photochem. Photobiol., B* **1998**, *44*, 191–198.
- Ravanat, J. L.; Douki, T.; Cadet, J. *J. Photochem. Photobiol., B* **2001**, *63*, 88–102.
- Prado Fernanda, M.; Oliveira Mauricio, C. B.; Miyamoto, S.; Martinez Glauca, R.; Medeiros Marisa, H. G.; Ronsein Graziella, E.; Mascio Paolo Di, *Free Radical Biol. Med.* **2009**, *47*, 401–409.
- Wang, S. Y.; Hahn, B. S.; Batzinger, R. P.; Bueding, E. *Biochem. Biophys. Res. Commun.* **1979**, *89*, 259.
- Beck, A. D. *J. Chem. Phys.* **1993**, *98*, 5648–5652.
- Parr, R. G.; Yang, W. *Density-Functional Theory of Atoms and Molecules*; Oxford University Press: Oxford, U.K., 1989.
- Przybylski, J. L.; Wetmore, S. D. *J. Phys. Chem. B* **2009**, *113*, 6533–6542.
- Millen, A. L.; Archibald, L. A. B.; Hunter, K. C.; Wetmore, S. D. *J. Phys. Chem. B* **2007**, *111*, 3800–3812.
- Wu, Y.; Xue, Y.; Xie, D.; Kim, C. K.; Yan, G. *J. Phys. Chem. B* **2007**, *111*, 2357.
- Mujika, J. I.; Formoso, E.; Mercero, J. M.; Lopez, X. *J. Phys. Chem. B* **2006**, *110*, 15000.
- Mujika, J. I.; Mercero, J. M.; Lopez, X. *J. Am. Chem. Soc.* **2005**, *127*, 4445.
- Manojkumar, T. K.; Suh, S. B.; Oh, K. S.; Cho, S. J.; Cui, C.; Zhang, X.; Kim, K. S. *J. Org. Chem.* **2005**, *70*, 2651.
- Yi, G. Q.; Zeng, Y.; Xia, X. F.; Xue, Y.; Kim, C. K.; Yan, G. S. *Chem. Phys.* **2008**, *345*, 73.
- Zhang, L.; Xie, D.; Xu, D.; Guo, H. *Chem. Commun.* **2007**, 1638.
- Jin, L.; Xue, Y.; Zhang, H.; Kim, C. K.; Xie, D. Q.; Yan, G. S. *J. Phys. Chem. A* **2008**, *112*, 4501.
- Wu, Y.; Jin, L.; Xue, Y.; Xie, D.; Kim, C. K.; Guo, Y.; Yan, G. *J. Comput. Chem.* **2008**, *29*, 1222.
- Almatarneh, M. H.; Flinn, C. G.; Poirier, R. A. *J. Phys. Chem. A* **2006**, *110*, 8227.
- Zeng, Y.; Xue, Y.; Yan, G. S. *J. Phys. Chem. B* **2008**, *112*, 10659–10667.
- Zhang, Q.; Bell, R.; Truong, T. N. *J. Phys. Chem.* **1995**, *99*, 592–600.
- Gonzalez, C.; Schlegel, H. B. *J. Chem. Phys.* **1989**, *90*, 2154–2161.
- Barone, V.; Cossi, M. *J. Phys. Chem. A* **1998**, *102*, 1995–2001.
- Cossi, M.; Rega, N.; Scalmani, G.; Barone, V. *J. Comput. Chem.* **2003**, *24*, 669–681.
- Frisch, M. J.; Trucks, G. W.; Schlegel, H. B.; Scuseria, G. E.; Robb, M. A.; Cheeseman, J. R.; Zakrzewski, V. G.; Montgomery, J. A., Jr.; Stratmann, R. E.; Burant, J. C.; Dapprich, S.; Millam, J. M.; Daniels, A. D.; Kudin, K. N.; Strain, M. C.; Farkas, O.; Tomasi, J.; Barone, V.; Cossi, M.; Cammi, R.; Mennucci, B.; Pomelli, C.; Adamo, C.; Clifford, S.; Ochterski, J.; Petersson, G. A.; Ayala, P. Y.; Cui, Q.; Morokuma, K.; Malick, D. K.; Rabuck, A. D.; Raghavachari, K.; Foresman, J. B.; Cioslowski, J.; Ortiz, J. V.; Stefanov, B. B.; Liu, G.; Liashenko, A.; Piskorz, P.; Komaromi, I.; Gomperts, R.; Martin, R. L.; Fox, D. J.; Keith, T.; Al-Laham, M. A.; Peng, C. Y.; Nanayakkara, A.; Gonzalez, C.; Challacombe, M.; Gill, P. M. W.; Johnson, B.; Chen, W.; Wong, M. W.; Andres, J. L.; Gonzalez, C.; Head-Gordon, M.; Replogle, E. S.; Pople, J. A. *Gaussian 03*, revision D.01; Gaussian, Inc.: Pittsburgh, PA, 2005.

- (44) Chen, Z. Q.; Zhang, C. H.; Xue, Y. *J. Phys. Chem. B* **2009**, *113*, 10409–10420.
- (45) Hruska, F. E.; Sebastian, R.; Grand, A.; Voituriez, L.; Cadet, J. *Can. J. Chem.* **1987**, *65*, 2618–2623.
- (46) Grand, A.; Cadet, J. *Acta Crystallogr.* **1978**, *B34*, 1524–1528.
- (47) Flippin, J. L. *Acta Crystallogr.* **1973**, *B29*, 1756–1762.
- (48) Although IRCs for the first and second steps should ideally lead to the same intermediate complex, two structures, A-PC1 and A1-PC1, with different water orientations were obtained. Considering the steric hindrance, it is more favorable for the water molecule to attack the C6 atom at the opposition of the C5 methyl group. Since we expect a low barrier for the ring-opening reaction, the energy barriers of steps 1 and 2 were discussed separately.
- (49) Note that A2-PC1 has one more water molecule than A-PC1, which has no effect on our results because it is the relative energy barriers that are used in our results.
- (50) Schweibert, M. C.; Daniels, M. *Int. J. Radiat. Phys. Chem.* **1971**, *3*, 353–336.
- (51) Cadet, J.; Téoule, R. *Biochim. Biophys. Acta* **1971**, *283*, 8–26.
- (52) Aruoma, O. I.; Halliwell, B.; Gajewski, E.; Dizdaroglu, M. *Biochem. J.* **1991**, *273*, 601–604.
- (53) Frew, J. E.; Jones, P.; Scholes, G. In *Mechanisms of DNA Damage and Repair*; Grossman, L., Upton, A. C., Eds.; Plenum Press: New York, 1986; pp 61–67.

JP100933D